Novel Multi-Coupled Line Resonators Replace Traditional Ceramic Resonators in Oscillators/VCOs

Ulrich L. Rohde, *Fellow, IEEE*
Synergy Microwave Corporation
Paterson, NJ 07504, USA
ulr@synergymwave.com

Ajay K. Poddar, *Senior Member, IEEE*
Synergy Microwave Corporation
Paterson, NJ 07504, USA
akpoddar@synergymwave.com

***Abstract*—Communication systems rely on stable signal source (Oscillator/VCO) to maintain phase-locked conditions and ensure transmitted data integrity. Many third and later generation systems incorporate multiple narrowband ceramic coaxial resonator oscillators (CROs) to cover their bandwidth requirement. Ceramic CROs are renowned for their ability to generate high spectral purity signal at RF/microwave frequencies. Unfortunately, CROs have several disadvantages, including a limiting temperature range, limited tuning range, not amenable for fabrication by current integrated circuit (IC) technology, and also sensitive to phase hits. These resonators are custom made for long lead-time and because of tension in crystal structure of the pressed and backed device, tend to cause phase hits in oscillators and synthesizers. This paper discusses the novel MCLR (multi-coupled line resonator) based oscillator/VCO, which is promising alternative of CROs, and supports better noise performance than commercial available high *Q* (quality factor) ceramic CROs at a fraction of cost.**

***Index Terms*—CRO, IC, MCLR, Phase Hits, Q, VCO**

I. INTRODUCTION

One of the largest growth areas in RF over the past decade has undoubtedly been in the applications of mobile communication system, and it's ever growing demand has caused renewed interest in and generated more attention towards wireless architectures and applications. Mobile phones and radios operating in several modes are typically switch between receiving frequencies and transmitting frequencies, and therefore, require low phase noise signal sources (Oscillators/VCOs) in each of the switched band. Using multiple self contained VCO (voltage controlled oscillator) has the disadvantage that it requires a substantial circuitry and valuable place on PCB (printed circuit board) viz. a complete set of self contained VCOs needed for different frequency band, each complete with phase locked loop. It would therefore be desirable to eliminate the need for multiple VCO's in multi-mode, multi-standard, and multi-band mobile phones. There are several different frequencies bands allocated for the modern mobile communication, but the most commonly used are located at approximately 450 MHz, 900 MHz, 1800 MHz, 1900 MHz, 2100 MHz, 2500 MHz and 5000 MHz. In order to give the user more freedom, phones that are able to cover more than one of these bands, require user defined high spectral purity signal source (oscillator/VCOs) that obviates the need for several phones, for each of which coverage would have to be checked when trying to communicate globally.

Oscillators/VCOs are the critical modules for virtually any communications, navigation, surveillance or test and measuring system. Despite the continuous improvement in the oscillators/VCOs technology, they still remain mysterious circuit modules and pose the main challenge due to the most demanding parameters such as low power consumption, minimal phase noise, low thermal drift, low phase hits, integrable, and compact size. The designer is continually asked to make tradeoffs between output power, power consumption, noise performance, stability, tuning range, interference immunity (sensitive to phase hits), size, and cost considerations [1-10]. Constraints on phase noise and broadband tunability are particularly demanding and a phase hits free solution has been the dream for decades.

Phase hits are infrequent but damaging causes of signal degradation in high-performance communication systems, and therefore effect increases with data rate and can un-lock many communication links if they cannot be absorbed. As a result, the continuing traffic are making phase hits a prime target for elimination. While phase hits have plagued communication equipments for years, today's higher transmission speeds accentuate the problem because of the greater amounts of data affected in a given time period. Thus, there exists a need for a method, which overcomes the above difficulties, and minimizes the phase hits of CROs, and integrable with the current IC fabrication technology.

The performance of communication system depends on the speed of the device, and typically specified by two figures-of-merit (FOM), such as transistor cutoff frequency f_T, and the maximum oscillation frequency f_{max}, which are defined as the frequency point where the current gain and

This work was supported in part by the U.S. government (DARPA and U.S Army).

1-4244-0074-0/06/$20.00 © 2006 IEEE.

the power gain become unity, respectively. The f_T and f_{max} for active device (SiGe HBT) is given by [4]

$$f_T \cong \frac{1}{2}\left[\frac{1}{g_m}(C_{be}+C_{cb})+\tau_b+\tau_e+\tau_{bc}\right]^{-1}, \quad f_{\max} \cong \sqrt{\frac{f_t}{8\pi R_b C_{cb}}} \quad (1)$$

where C_{be} is the parasitic emitter-base junction capacitance, C_{bc} is the parasitic collector-base junction capacitance, R_b is the parasitic base resistance, g_m is the device transconductance, τ_b is the base transit time, τ_e is the emitter delay time, and τ_{bc} is the base-collector junction depletion layer time.

For high speed and low noise RF and microwave applications, the transistor geometric profile of the SiGe HBTs need to be properly scaled and optimized to the minimum noise figure for low phase noise applications [3,4]. Therefore, more and more applications push the boundaries of the VCO's design to the limit of the physics.

The above limitation has made it to explore and pursue other alternative approaches such as N-Push VCO, RF-MEMS (Radio-Frequency Micro-Electro Mechanical-System) VCO, OE (Opto-Electronic) VCO, YIG (Yttrium-Iron-Garnet) VCO, SAW (Surface acoustic wave) VCO, and CRO (Coaxial resonator oscillator), and planar resonator (Microstripline/Stripline) based oscillator topologies [1-16].

The N-Push coupled VCO topology extends the frequency generation capabilities of the active device (bipolar/FETs) beyond the limitation caused by the f_T and f_{max} for active device, and minimizes the phase noise in comparison with the single individual uncoupled oscillator by the factor N, where 'N' is the number of uncoupled oscillator modules in N-Push domain [2]. The drawback of N-Push approach is the complicated design and mismatch in phase-shift between the successive oscillators circuits in N-Push configuration [3].

RF-MEMS based VCO's components such as inductors, variable capacitors, and resonators are superior in performances in term of quality factor, noise, linearity, power consumption, size, and cost, which cannot be achieved by conventional approach, thereby, makes promising alternative and prime candidate for wireless connectivity. However, MEMS devices, unlike ICs, contain moving fragile parts that must be properly packaged and meet the requirements such as protection against handling, shielding against electromagnetic fields, near hermetic cavity seal, low temperature process, good heat-exchange, minimal thermal stress, and RF electrical feed through before it becomes commercial viable alternatives [5,15,16].

The OEO is a hybrid feedback oscillator, which converts optical energy from a laser to microwave/millimeter wave, and exhibits spectral purity signals but the major challenge in the OEO is mode locking, and circuit has to operate in a single mode from those available natural multi-modes [13].

YIG ($Y_3Fe_5O_{11}$) oscillators are known for low noise broadband signal source but at the cost of size, power and integrability in IC (integrated circuit) form. In addition to this, YIG is sensitive to vibration, lighting, electromagnetic interference (EMI), microphonics, phase hits, and frequency modulation, all of which have a detrimental effect in designing modern communication systems [12,14].

SAW (surface acoustic wave) oscillators are well known for high spectral pure stable reference signal sources (Oscillators/VCOs). SAW oscillators utilizing high Q lithium niobate devices as a two-port resonator used in oscillator/VCOs and they have a very small pulling range, which does not support sufficient tuning range to compensate all the tolerance due to the device package parasitics, circuit components and thermal drift over the required operating temperature range. Besides these, SAW device are comparatively expensive and prone to microphonics, and its availability and performances are limited to selected frequency and temperature range, therefore, not suitable for operating in stringent temperature environment and also low cost applications [6,11,12,14].

CROs (coaxial resonator oscillators) are based on high Q ceramic resonators, and cost-effective alternative of SAW VCOs. Unfortunately, CROs oscillators have several disadvantages, including a not integrable with present fabrication technology, limiting temperature range, limited tuning range (which limits the amount of correction that can be made to compensate for the tolerances of other components in the oscillator circuit), and sensitive to phase hits (due to expanding and contracting at different rates with variation of the temperature for outer metallic body of the CROs and other components of the oscillator circuit) [8,9].

Microstripline resonator based oscillators/VCOs are planar circuits and easily amenable for integration in IC form but offers poor phase noise performance in comparison to above discussed other resonator-based oscillator/VCOs. Microstripline resonator exhibits low quality factor and the resonant frequency is dependent on the length of the resonators, thereby, leads to degradation in the Q factor if the same structure is used for other frequency band [11-14].

Standard integrated circuits are planar circuits, so only those resonators having a planar structure are suitable for designing a microwave integrated circuit (MMIC) or radio frequency integrated circuit (RFIC). The object of the present work is to provide user defined single high purity signal source for the several different frequency bands allocated for present and later generation wireless systems, which otherwise needed several signal sources to meet the same requirement. The new approach is based on noise cancellation technology utilizing MCLR (Multi-coupled line resonator) in which the total dimensions of the resonator is unaltered and at the same time it exhibits multi-band resonance without degradation of the Q factor, thereby, reduction in the number of manufacturing process steps [1].

II. THEORY

A principal goal of the present work is to replace traditional ceramic resonators in oscillators/VCOs and provide a manufacturable method for generating high

spectral purity oscillator, which is compact and amenable for integration in chip form. Ceramic CROs (coaxial resonator oscillators) are widely used in wireless applications, since the technology features very low phase noise at fixed frequencies through about 4000 MHz. Ceramic resonator based oscillators are also known for high quality factor (Q), and low phase noise performances. Typically, a ceramic resonator comprises a dielectric material formed as a rectangle prism with a coaxial hole running lengthwise through the prism and an electrical connector connected to one end. The outer and inner surfaces of the prism, with the exception of the end connected to the electrical connector and possibly the opposite end, are coated with a metal such as copper or silver. A device formed in this manner forms a resonant RF circuit, including capacitance, inductance, and loss resistance that oscillates in the transverse electromagnetic (TEM) mode, if loss resistance is compensated. The advantages gained with this design include a high quality factor (Q), and therefore, exhibits low phase noise.

Unfortunately, CROs have several disadvantages, including a limiting temperature range, limited tuning range (which limits the amount of correction that can be made to compensate for the tolerances of other components in the oscillator circuit), and sensitive to phase hits (due to expanding and contracting at different rates with variation of the temperature for outer metallic body of the coaxial ceramic resonator and other components of the oscillator circuit). Therefore, due diligence must be done upfront by the designer considering using a digitally implemented CROs oscillator to over come the above problems, otherwise, large phase hits can un-lock many communication links if it is not absorbed. In addition, since the design of a new CROs oscillator is much like that of an integrated circuit (IC), development of an oscillator with a non standard frequency requires nonrecurring engineering (NRE), in addition to the cost of the oscillators [8,12,14].

Phase hits can be defined as sudden, uncontrolled changes in the phase of the signal source that occurs randomly, and generally lasts for fractions of a second [12]. It can be caused by temperature changes from dissimilar metals expanding and contracting at different rates, as well as from vibration or impact. Microphonics, which are acoustic vibrations that traverse an oscillator package and circuits and cause change in phase and frequency, are dealt with present work through novel topology (patent pending) by using hybrid resonance mode in distributed planar MCLR (Multi-coupled line resonator). Oscillators/VCOs can be divided into many different types based on tuning range, type of resonators active device used. Resonators largely determine frequency tuning range, stability and noise performance of the oscillator, and are commonly used to nomenclature the different types of oscillators/VCOs.

A. Resonator

A resonator is an important element in oscillator/VCO and its characteristics are based on size, cost, quality factor, manufacturability and integrability. Some common microwave resonators (LC, Ceramic, Cavity, Dielectric, SLC, BAW, OE, YIG, Microstripline) are discussed for comparative analysis with reference to their integrability and applications in oscillators/VCOs. LC resonator is formed by a plurality of inductors and capacitors, exhibits low Q factor because of the large value of loss resistance. Ceramic coaxial resonator is high Q resonator but large, expensive, and not amenable for integration in IC form. Cavity resonator (formed of conductive materials in different shape: rectangular, cylindrical or spherical shape) is high Q resonator, and has characteristics of low power consumption but they are impractical due to the large size of cavities, therefore, restricted application in signal generation. Dielectric resonators are made of $BaTi_4O_9$ and Z_rSnTiO_4, resonate in various modes ($TE_{01\delta}$ mode is used for the optimum temperature stability) and exhibit high Q factor but costly and not useful below 2GHz frequency of operation. Sapphire-loaded cavity resonator (SLC) is a low loss dielectric material (sapphire), exhibits high Q factor (by using whispering gallery modes) but costly, therefore, restricted applications. Bulk acoustic wave (BAW) resonators are a three-layer structure (with the top and bottom electrodes of molybdenum sandwiching a middle layer of oriented piezoelectric aluminum nitride) exhibit reasonable good Q factor but sensitive to temperature and needed thermal stabilization before it can be exploited commercially. Optoelectronic (OE) resonator uses optic resonator system for the exceptionally high Q factor. OE resonator supports phase noise performance independent of frequency that enables the generation of a low phase noise signal from microwave to millimeter wave but its application is limited due to multi-mode operation resulting in gaps in the frequency coverage as well as relatively high spurs. YIG resonator is made of yttrium iron garnet ($Y_3Fe_5O_{11}$), exhibits high Q factor but its application is limited to operating frequency (at higher frequency due to the magnetic saturation and high power dissipation, and the at lower frequency limited by the saturation magnetization $4\pi Ms$). The last resonator is a planar microstripline resonator is formed by disposing a conductive strip onto a circuit board, which is cost-effective and amenable for integration in IC form but at the cost of large size and low Q factor in comparison to the other discussed resonators.

Standard integrated circuits are planar circuits, therefore effort is to eliminate discrete and bulky resonators, and produce high Q planar resonators by exploring new techniques such as coupled resonator configuration for low noise signal sources (oscillators/VCOs) [1, 3,7, 11, 12].

B. Coupled Resonators

The Q factor of the resonator network can be improved by introducing coupling mechanism (inductive/capacitive/ mode-coupling). For better insights about the improvement in the Q factor, Fig.1 illustrates the typical capacitive coupling mechanism between two identical resonators. As shown in Fig.1, the resonators are represented by equivalent parallel RLC network, where Z_r and Z_c are the resonators and the coupling network impedance, respectively [1-4].

The coupling factor β of the coupled resonator network (Fig.1) is defined as the ratio of the series coupling capacitor (C_c) to the resonator capacitor (C). The effective coupled impedance (Fig. 1) is given by [1,3]

$$Z_{eff}(\omega)=\left[\frac{V_o}{I_{in}}\right]=\frac{Z_r(\omega)}{2+\dfrac{Z_c(\omega)}{Z_r(\omega)}}=\frac{Z_r^2(\omega)}{Z_c(\omega)+2Z_r(\omega)} \tag{2}$$

$$Y_{eff}(\omega)=\frac{1}{Z_{eff}(\omega)}=\left[\frac{Z_c(\omega)}{Z_r^2(\omega)}+\frac{2}{Z_r(\omega)}\right]=\left[\frac{Y_r^2(\omega)}{Y_c(\omega)}+2Y_r(\omega\right] \tag{3}$$

Where I_{in} is the large signal current from the active device (Bipolar/FET). For $Z_c(\omega)>>Z_r(\omega)$, and assuming the Q factor of $Z_r(\omega)$ is sufficiently large, the denominator of (2) can be considered as uniform over the frequencies within the bandwidth of $Z_r(\omega)$. The coupling admittance is defined by $Y_c(\omega)=j\omega C_c$. The resonator admittance is given by

$$Y_r(\omega)=\left[\frac{1}{R_P}+\frac{1}{j\omega L}+j\omega C\right]=\left[\frac{j\omega LR_P}{R_P(1-\omega^2LC)+j\omega L}\right]^{-1} \tag{4}$$

$$Y_{eff}(\omega)=\left[\frac{2}{R_P}-\frac{2R_P(1-\omega^2LC)}{\omega^2LR_P^2\beta C}\right]+j\left[\frac{[R_P^2(1-\omega^2LC)^2-\omega^2L^2]}{\omega^3R_P^2L^2\beta C}-\frac{2R_P(1-\omega^2LC)}{R_P\omega L}\right] \tag{5}$$

From (5), the phase shift of the coupled resonator is

$$\varphi=\tan^{-1}\left[\frac{\left(\dfrac{[R_P^2(1-\omega^2LC)^2-\omega^2L^2]}{\omega^3R_P^2L^2\beta C}-\dfrac{2R_P(1-\omega^2LC)}{R_P\omega L}\right)}{\left(\dfrac{2}{R_P}-\dfrac{2R_P(1-\omega^2LC)}{\omega^2LR_P^2\beta C}\right)}\right] \tag{6}$$

At resonance the real part of $Y_{eff}(\omega)$ is reduced to zero, and the resonance frequency can be given by

$$\mathrm{Re}[Y_{eff}(\omega)]_{\omega=\omega_0}=\left[\frac{2}{R_P}-\frac{2R_P(1-\omega^2LC)}{\omega^2LR_P^2\beta C}\right]_{\omega=\omega_0}=0\Rightarrow\omega_0^2LC(1+\beta)=1 \tag{7}$$

$$[\omega_0]_{\phi=90^0}=\frac{1}{\sqrt{LC(1+\beta)}};\quad [Y_{eff}(\omega)]_{\omega=\omega_0}=-j\left[\frac{R_P^2\beta^2C+(1+\beta)L}{\beta(1+\beta)\omega LR_P^2C}\right] \tag{8}$$

$$Z_{eff}(\omega)]_{\omega=\omega_0}=j\left[\frac{\beta(1+\beta)\omega LR_P^2C}{R_P^2\beta^2C+(1+\beta)L}\right]=j\left[\frac{\beta R_P^2\omega C}{\dfrac{R_P^2\beta^2C}{(1+\beta)L}+1}\right]\Rightarrow j\left[\frac{Q_0\beta R_P}{1+Q^2\beta^2}\right] \tag{9}$$

where

$$Q_0(uncoupled)=\omega CR_P=\frac{R_P}{\omega L};\ \beta=\frac{C_c}{C}$$

From (6), the quality factor of the capacitive coupled resonator network as shown in Figure 1 is given by

$$[Q_{coupled}(\omega)]_{\omega=\omega_0}=\frac{\omega_0}{2}\left[\frac{\partial\phi}{\partial\omega}\right]\Rightarrow\frac{2Q_0(1+\beta)}{(1+Q_0^2\beta^2)}\rightarrow\left[\frac{2Q_0(1+\beta)}{(1+Q_0^2\beta^2)}\right]_{\beta<<1}\approx 2Q_0 \tag{10}$$

From (9) and (10), for weak coupling (β<<1), attenuation is high due the large value of Z_c, therefore, there is trade-off between doubling the Q factor and the permissible attenuation required for the minimum phase noise performance. For wideband tunability, the coupling factor β, is dynamically adjusted over the tuning range by varying the coupling capacitor C_C by using tuning diode for low noise performance over the required tuning range.

Figure 2 shows the schematic of the 1000 MHz coupled based oscillator for giving insight into the reduction of the phase noise with respect to the uncoupled single ceramic resonator oscillator. Figure 3 shows the transistor (NE 68830) with the package parameters for the calculation of the oscillator frequency. Table1 shows the transistor spice and package parameters of NE68830 from manufacturer (NEC) data sheets. The frequency of the oscillation for the oscillator circuit shown in Figure 2 is given by [1,3]

$$\omega_0=\sqrt{\left\{\frac{\left(\dfrac{(C_1^*+C_P)C_2}{(C_1^*+C_P+C_2)}+C_{c1}\right)}{L_{PR}\left[\left(\dfrac{(C_1^*+C_P)C_2C_{c1}}{(C_1^*+C_P+C_2)}\right)+C_{PR}\left(\dfrac{(C_1^*+C_P)C_2}{(C_1^*+C_P+C_2)}+C_{c1}\right)\right]}\right\}}\approx 1000MHz \tag{11}$$

with C_1^*= 2.2pF, C_1= C_1^*+C_P, C_P=1.1pF (C_{BEPKG} + contribution from layout), C_2 = 2.2pF, C_{c1} = 0.4pF; Resonator: R_{PR} =12000Ω, C_{PR} = 4.7pF, L_{PR} =5nH

Figure 4 shows the CAD simulated (Ansoft Designer) response of the coupled resonators oscillator circuit having resonance at 999.9 MHz, or a less than 1% error. The variation in resonant frequency may be due to the frequency dependent packaged parameters, but it is a good starting value for the analysis of the coupled resonator-based oscillator. Figs. 5 and 6 demonstrate the simulated and the measured phase noise plot for the single resonator and the identical coupled resonator (2-resonators); simulated and measured phase noise data agree within 1-3 dB.

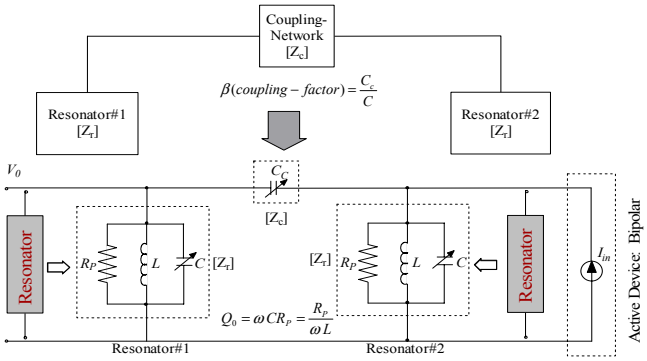

Fig.1. Typical capacitive coupled resonator oscillator

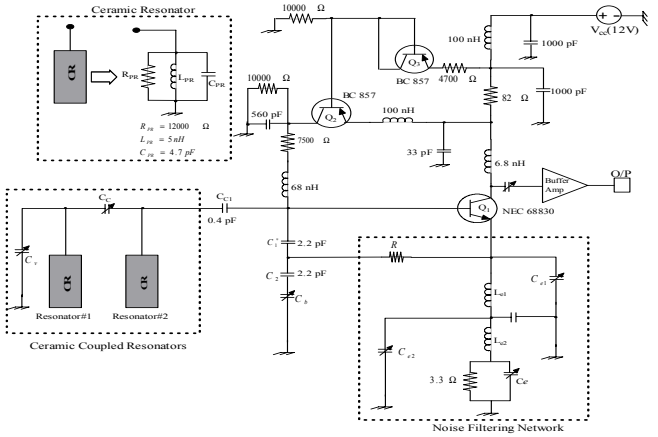

Fig. 2. 1000 MHz parallel-coupled resonator oscillator (patent pending)

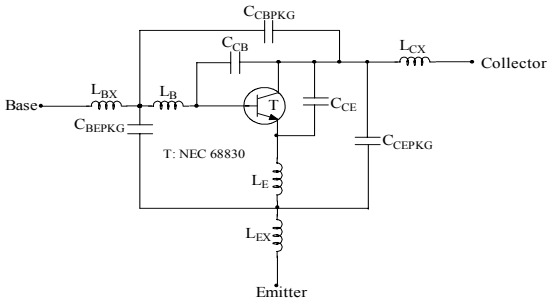

Figure 3. NE68830 with package parasitics (T: intrinsic transistor)

Table 1. Spice parameters (Gummel- Poon Model, Berkley-Spice)

Parameters	T (NEC)	Parameters	T (NEC)	Packages	T (NEC)
IS	3.8E-16	MJC	0.48	C_{CB}	0.24E-12
BF	135.7	XCJC	0.56	C_{CE}	0.27E-12
NF	1	CJS	0	L_B	0.5E-9
VAF	28	VJS	0.75	L_E	0.86E-9
IKF	0.6	MJS	0	C_{CBPKG}	0.08E-12
NE	1.49	TF	11E-12	C_{CEPKG}	0.04E-12
BR	12.3	XTF	0.36	C_{BEPKG}	0.04E-12
NR	1.1	VTF	0.65	L_{BX}	0.2E-9
VAR	3.5	ITF	0.61	L_{CX}	0.1E-9
IKR	0.06	PTF	50	L_{EX}	0.2E-9
ISC	3.5E-16	TR	32E-12		
NC	1.62	EG	1.11		
RE	0.4	XTB	0		
RC	4.2	KF	0		
CJE	0.79E-12	AF	1		
CJC	0.549E-12	VJE	0.71		
XTI	3	RB	6.14		
RBM	3.5	RC	4.2		
IRB	0.001	CJE	0.79E-12		
CJC	0.549E-12	MJE	0.38		
VJC	0.65				

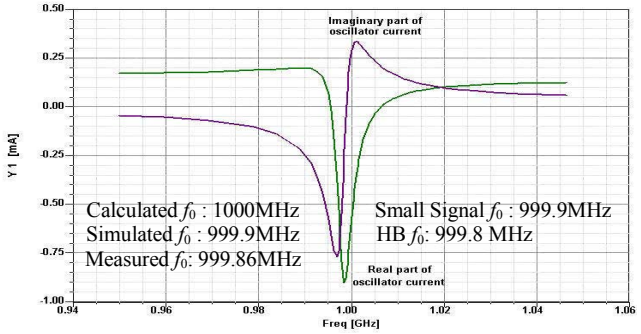

Fig. 4. Simulated response of the real and imaginary part of RF current of oscillation for oscillator circuit shown in Fig. 2

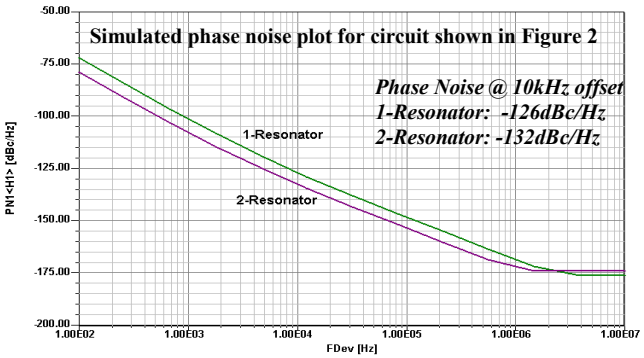

Fig.5. Simulated phase noise plot for the single resonator (1-resonator) and the identical coupled resonator (2-resonators); CROs

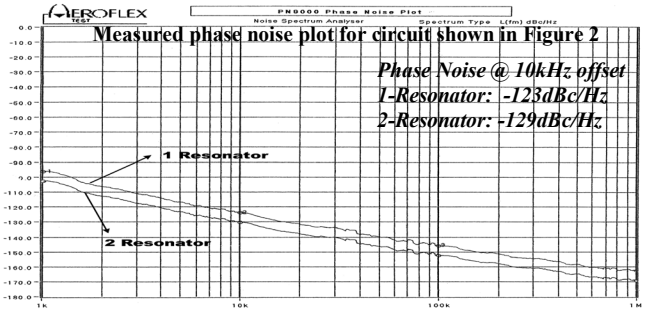

Figure 6. Measured phase noise plots for the single resonator (1-resonator) and the identical coupled resonator (2-resonators)

C. *Thermal Drift Profile and Tuning Range in CROs*

Figure 7 illustrates the typical example of thermal drift profile and frequency tuning range for a ceramic resonator based oscillators (as shown in Figure 2). Figures 8 and 9 show the novel approach for minimization of the thermal drift by incorporating slot-cut distributed planar medium coupled with the ceramic resonators that works as a evanescent mode buffer between the tuning network and the active device to comensate for changes in the component parameters of the passive and active devices caused due to change in temperature during operation. Based on patent pending approach, thermal drift profile of the CROs can be defined apriori, and also can be mimimized by selecting optimum ratio of l_1/w and l_2/w for a given dielectric constant ε_{r1}, ε_{r2}, operating frequency, and physical dimensions (width: w, height: h, length: l_1, l_2, slot: d) as illustrated in Figures 8 and 9. Figures 10 and 11 show schematic of the ulow thermal drift oscillator circuit and mesaured data for frequency drift (with and without evanescent mode buffer) due to change in operating temperature.

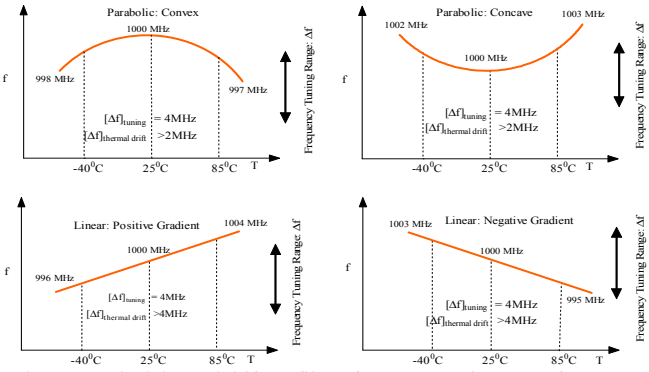

Fig. 7. Typical thermal drift profile & frequency tuning range for CROs

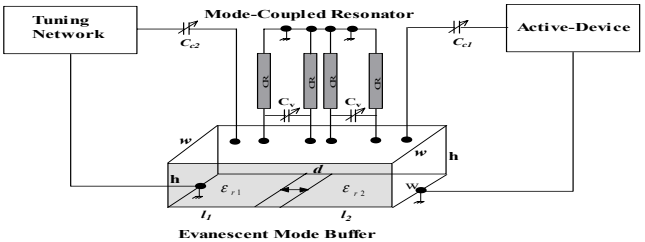

Fig.8. Novel approach for minimization of frequency drift due to change in temperature (patent pending)

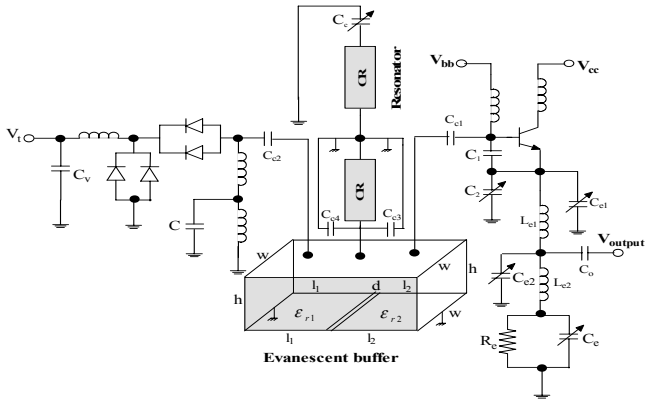

Fig.9. Typical example of CROs for minimization of frequency drift due to change in temperature (patent-pending)

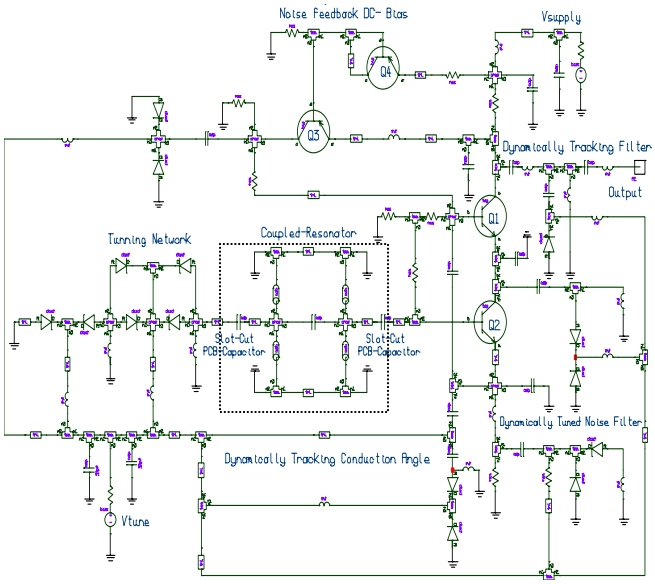

Fig.10. Schematic of 1000 MHz coupled CROs circuit using evanescent mode buffer (slot-cut PCB-Capacitor)

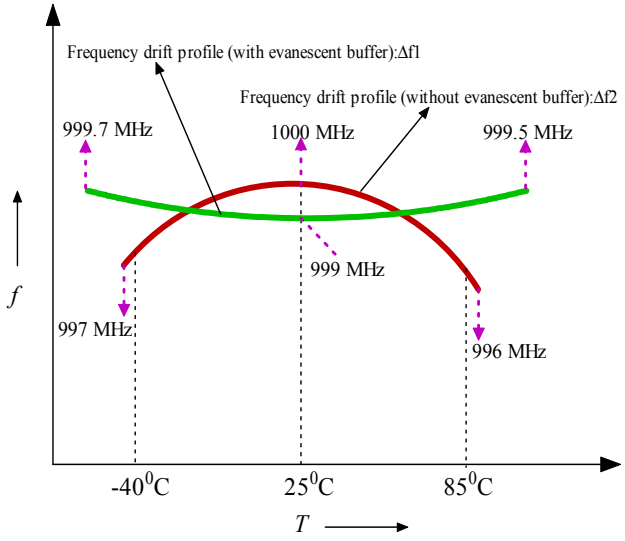

Fig.11. Measured thermal profile for circuit shown in Figure 10 (with and without evanescent buffer); Δf2>Δf1

D. *MCLR* (*Multi-Coupled Line Resonators*) *VCO*

An object of this work was to replace the CROs by improving the *Q* value of the microstripline resonator by cascading a plurality of resonating network such as MCLR having multiple asymmetric coupled line to increase the phase derivative and group delay [δφ/δω] of the resonator in a given cycle (9). Therefore, oscillators/VCOs circuit is designed such that the phase condition occurs in the steepest part of the phase characteristics curve of the planar-coupled resonators. In this way, coupled mode resonance may substantially coincide with a maximum-slope of the phase characteristic curve of the oscillator circuit, and the operation of the oscillator circuit about this point results in the circuit operating within the lowest phase noise domain of the phase characteristic curve, thereby improved effective dynamic loaded *Q* [1-3]. Figs. 12 and 13 show the block diagram and layout of wideband MCLR VCO (500 MHz-2500 MHz), which is based on novel topology that supports broadband tunability for compensating the frequency drift due to temperature and ageing that offers user definable frequency band in compact size ($0.75'' \times 0.75''$) and amenable for integration in the IC (integrated circuit) form.

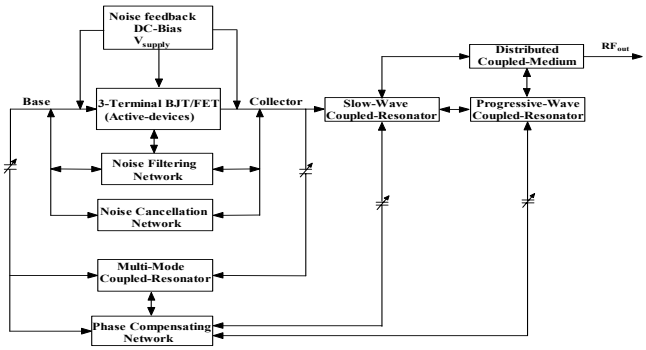

Fig. 12. Block diagram of the wideband MCLR VCO (Patent pending)

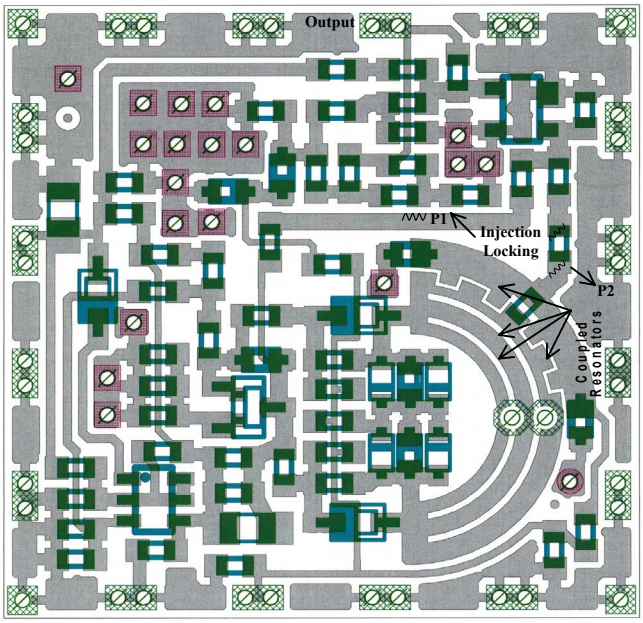

Fig. 13. Layout of the MCLR VCO (500MHz-2500MHz) (Patent pending)

Fig. 14 illustrates the measured Q of the typical planar-coupled resonators (uncoupled, coupled, MCLR) for the purpose of comparative analysis [1,3]. For minimum noise performance, oscillator circuit shown in Figure 13, works on self-injection locking mode, where signal P1 acts like as a reference input signal to RF signal P2 (as shown in Fig.13) that is coupled through a distributed medium for broadband (500-2500MHz) tuning and minimum noise performance.

E. Tuning Characetristics

The resistive loading and package parasitic effects of the tuning diode limit the tuning range. Fig.15 shows the equivalent circuit model of the varactor-tuned VCO to show the tuning diode loading effect of the oscillator circuits. The varactor capacitance C_v is a function of the tuning voltage, which is decreasing monotonically from C_{V0} at zero bias to C_{VB} at breakdown. The capacitance ratio '*r*' is defined as the ratio of C_{V0} and C_{VB}. For simplification, the series resistance R_s given in Fig. 15 is assumed to be constant at all bias levels. The equivalent parallel representation of resistance R_P, capacitance C_p and quality factor Q_v of series tuning diode (varactor) shown in Fig.15 is given by [3]

$$R_p = R_s\left[1+Q_v^2\left(\frac{C_{v0}}{C_v}\right)^2\right] \cong R_s Q_v^2\left(\frac{C_{v0}}{C_v}\right)^2; \quad for\ \ Q_v >> 1 \tag{12}$$

$$C_{vp} = \frac{C_{vs}}{\left[1+\frac{1}{Q_v^2}\left(\frac{C_v}{C_{v0}}\right)^2\right]} \cong C_{vs}, \quad Q_v = \frac{1}{\omega R_s C_V}; \quad for\ \ Q_v >> 1 \tag{13}$$

Without tuning diode, the resonant frequency and unloaded Q (Q_0) of the oscillator is given by (for $|-R_n| = R_L$)

$$\omega_0 = \sqrt{\frac{1}{LC}}, \quad Q_0 = \omega_0 CR \tag{14}$$

With tuning diode, the frequency of the oscillation can be tuned from ω_1 to ω_2:

$$\omega_1 = \sqrt{\frac{1}{L(C+C_{v0})}}, \quad \omega_2 = \sqrt{\frac{1}{L(C+C_{VB})}} \tag{15}$$

The fractional tuning range with respect to ω_1 can be expressed as a function of the capacitance ratio as

$$\frac{\Delta f}{f_1} = \frac{\omega_2 - \omega_1}{\omega_1} \cong \frac{1}{2}\left[\frac{C_{V0} - C_{VB}}{C + C_{V0}}\right] = \frac{1}{2}\left[\frac{1-\frac{1}{r}}{1+\frac{C}{C_{V0}}}\right] \tag{16}$$

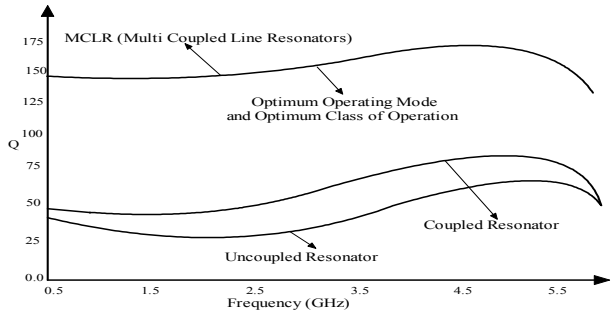

Fig. 14. Measured Q of planar resonators (uncoupled, coupled and MCLR)

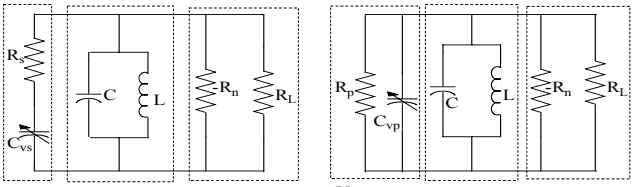

Fig.15. Equivalent circuit of the varactor tuned negative resistance oscillator with the tuning diode represented by (a) series RC circuit and (b) parallel RC circuit (without parasitics).

The loaded Q (Q_L) of the oscillator at zero bias is [3]

$$Q_L = \omega(C+C_{V0})\left[\frac{RR_sQ_v^2}{R+R_sQ_v^2}\right] = \left[\frac{Q_0Q_v^2}{\left(\frac{R}{R_s}\right)+Q_v^2} + \frac{Q_v}{1+\left(\frac{R_s}{R}\right)Q_v^2}\right] \tag{17}$$

$$\frac{Q_L}{Q_0} = \left[1+\left(2r\frac{\Delta f}{f_1}\right)\frac{\left(\frac{Q_0}{Q_v}-1\right)}{(r-1)}\right]^{-1} = \left[1+(2rp)\frac{(q-1)}{(r-1)}\right]^{-1} \tag{18}$$

where

$$p = \frac{\Delta f}{f_1},\ q = \frac{Q_0}{Q_v},\ r = \frac{C_{V0}}{C_{VB}} >,\ Q_v|_{v=0} = \frac{1}{\omega R_s C_{V0}},\ \ and\ \ Q_v|_{v=VB} = \frac{1}{\omega R_s C_{VB}}$$

From (17) and (18), the loaded Q of the varactor-tuned VCOs reaches its lowest value at zero tuning voltage because varactor at zero bias introduces the greatest perturbation and its own Q is at its lowest. The amount of loading on a resonator is critical for low phase noise in oscillators/VCOs.

F. Oscillator Phase Noise

The expression of the phase noise is given by [1,3]

$$£(f_m) = 10\log\left\{\left[1+\frac{f_0^2}{(2f_mQ_0)^2m^2(1-m)^2}\right]\left(1+\frac{f_c}{f_m}\right)\frac{FkT}{2P_0} + \frac{2kTRK_0^2}{f_m^2}\right\} \tag{19}$$

where m, Q_0, Q_L, f_0, f_c, f_m, F , K_0, R, k and T are defined as ratio of the loaded and unloaded Q, unloaded Q, loaded Q, oscillation frequency, flicker corner frequency, offset frequency from the carrier, noise factor, oscillator voltage gain, noise resistance of the tuning diode, Boltzman's constant and temperature in degree K.

From (19) minimum phase noise can be obtained by differentiating (19) with respect to m, and equating to zero,

$$\frac{d}{dm}\left[10\log\left\{\left[1+\frac{f_0^2}{(2f_mQ_0)^2m^2(1-m)^2}\right]\left(1+\frac{f_c}{f_m}\right)\frac{FkT}{2P_0} + \frac{2kTRK_0^2}{f_m^2}\right\}\right] = 0 \Rightarrow m_{opt} = 0.5 \tag{20}$$

From (19) and (20), as depicted in Fig.16, for different values of noise figure F ($F_3>F_2>F_1$), the phase noise is minimum at m_{opt}, and the plot is typically like 'bath-tub' curve, which is shifted symmetrically about m_{opt}. This implies that for low noise application, the value of m should be dynamically tuned over the tuning range and should lie in the vicinity of m_{opt} for minimum noise performance [1,3].

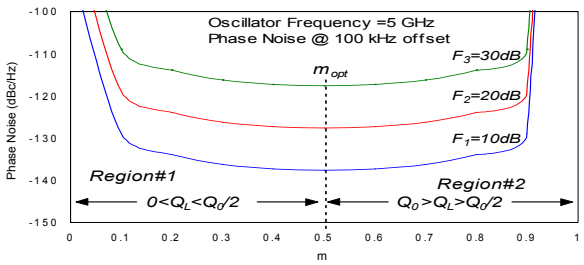

Fig. 16. Phase noise vs. m (Q_L/Q_o) of the resonator

III. NOISE ANALYSIS

The following noise analysis is based on the negative resistance and the feedback approach, is an attempt to introduce the concept of the reduction in the phase noise in terms of the oscillator operating condition and the circuit component parameters.

A. Noise Analysis Based On Negative Resistance Model

Fig. 17 shows the equivalent representation of negative resistance Colpitts oscillator with series tuned LC resonator and small signal AC equivalent circuit. The noise voltage $e_n(t)$ describes a small perturbation, which is the noise resulting from R_L and $-R_n(t)$. The time dependence of the negative resistance $R_n(t)$ comes from the fact that the collector current is a series of pulses and the negative resistance is only present during a small period of the time. The phase noise of the oscillator circuit (Fig.17) [3] is

$$\pounds(\omega) \cong 10Log\left\{\left[4kTR_L + \frac{4qI_c g_m^2 + \frac{K_f I_b^{AF}}{\omega} g_m^2}{\omega_0^2 C_1^2 (\omega_0^2 (\beta^+)^2 C_2^2 + g_m^2 \frac{C_2^2}{C_1^2})}\right]\left[\frac{\omega_0^2}{4\omega^2 V_{cc}^2}\right]\left[\frac{1}{Q_L^2} + \frac{[C_1+C_2]^2}{C_1^2 C_2^2 \omega_0^4 L^2}\right]\right\} \quad (21)$$

$$[\beta^+] \approx \left[\frac{Y_{21}^+}{Y_{11}^+}\right]\left[\frac{C_1}{C_2}\right]^{\alpha}; \quad g_m \approx [Y_{21}^+]\left[\frac{C_1}{C_2}\right]^{\gamma} \quad (22)$$

where Y_{21}^+, Y_{11}^+ is the large signal [Y] parameter of the active device, K_f is the flicker noise coefficient, AF is the flicker noise exponent, $\pounds(\omega)$ is the ratio of sideband power in a 1Hz BW at ω to total power in dB, ω is the offset frequency from the carrier, ω_0 is the resonance frequency, Q_L is the loaded Q of the tuned circuit, kT is the 4.1×10^{-21} at 300 K, R_L is the equivalent loss resistance of the tuned resonator circuit, I_c is the collector current, I_b is the base current, V_{cc} is the collector voltage, C_1, C_2 is the feedback capacitor (Fig.17), α and γ are the constant depend upon the drive level across base-emitter junction of the transistor.

To achieve the minimum possible phase noise level, the feedback capacitors C_1 and C_2 should be made as large as possible, but still generate sufficient negative resistance for sustaining steady-state oscillation. The negative resistance of the oscillator circuit is inversely proportional to the feedback capacitors; therefore, the minimum negative resistance for a loop gains greater than unity determines the limit of the feedback capacitor values. The negative resistance model provides design guide for the oscillator; however, it fails to provide the individual contribution of the noise sources of the oscillator circuit comprise of active and passive devices.

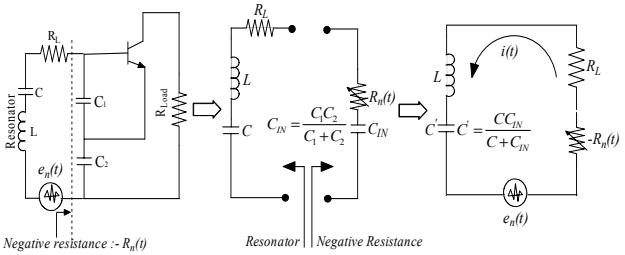

Fig. 17. Typical negative resistance oscillator circuit (without parasitics)

B. Noise Analysis Based On Feedback Model

Fig. 18 shows the feedback arrangement for the Colpitts oscillator with the following noise source of the oscillator: thermal noise associated with the loss resistance of the resonator i_{nr}, thermal noise associated with the base resistance of the transistor v_{bn}, shot noise associated with the base bias current i_{bn}, and the shot noise associated with the collector bias current i_{cn}. Based on this approach, the expression of the total phase noise (contribution due to the thermal noise associated with the loss resistance of the resonator R_P, thermal noise associated with the base resistance of the transistor r_b, shot noise associated with the base current, shot noise associated with the collector current, and the flicker noise associated with the transistor) can be given by $[PN(\omega_0+\omega)]_{total} = [PN_{inr} + PN_{Vbn} + PN_{icn} + PN_{ibn} + PN_{ifn}]$

$$[PN(\omega_0+\omega)]_{total} = \frac{4KT}{R_P}\left\{\frac{1}{2}\left[\frac{1}{2j\omega_0 C_{eff}}\right]\left[\frac{\omega_0}{\omega}\right]\right\}^2_{inr} + 4KTr_b\left\{\frac{1}{2}\left[\frac{C_1+C_2}{C_2}\right]\left[\frac{1}{2jQ}\right]\left[\frac{\omega_0}{\omega}\right]\right\}^2_{Vbn}$$

$$+2qI_c\left\{\frac{1}{2}\left[\frac{C_1}{C_1+C_2}\right]\left[\frac{1}{2j\omega_0 Q C_{eff}}\right]\left[\frac{\omega_0}{\omega}\right]\right\}^2_{icn} + \left[2qI_b + \frac{2\pi K_f I_b^{AF}}{\omega}\right]\left\{\frac{1}{2}\left[\frac{C_2}{C_1+C_2}\right]\left[\frac{1}{j2Q\omega_0 C_{eff}}\right]\left[\frac{\omega_0}{\omega}\right]\right\}^2_{ibn+ifn} \quad (23)$$

where $C_{eff} = C + \frac{C_1 C_2}{C_1+C_2}$, K_f is the flicker noise constant, AF is the flicker noise exponent, and ω is the offset frequency.

From (23), this approach allows us to derive explicit closed-form expression of the phase noise in terms of the individual contribution of the noise sources, oscillator circuit operating condition, and device circuit component parameters.

To test the validity of both the noise models, we build 1 GHz Colpitts oscillator (shown in Fig. 19) using high Q resonator (ceramic resonator). The phase noise contribution from the different noise sources for the circuit shown in the Fig.19 is computed and compared with the simulated and measured result. The layout of 1GHz oscillator as shown in Fig.19 is fabricated on 32mil thick Roger substrate of dielectric constant 3.38, and loss tangent $2.7X10^{-4}$.

The optimum circuit parameters for minimum phase noise performance for the oscillator circuit shown in the Figure 19 is given as: r_b = 6.14 Ω, R_P =12000 Ω, Q_L=380, L=5 nH, C = 4.7 pF, C_1=3.3 pF, C_2=2.2 pF, I_c=28 mA, I_b=250 uA, AF=2, K_f = 1E-9, α=1.1, and γ=1.5. To confirm the validity of the noise models (negative resistance and feedback model), we compare results of the simulation and measurement for the circuit shown in the Fig.19.

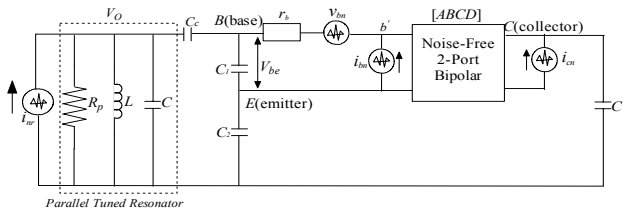

Fig. 18. Feedback model of the 1 GHz oscillator with the 2-port bipolar

From (21), negative resistance model, the calculated phase noise for circuit shown in Fig.19 @ 100Hz and 10kHz offset frequency from carrier is -70 *dBc/Hz*, and –126 *dBc/Hz* respectively, whereas, from (23), feedback model, the calculated phase noise is -68 *dBc/Hz*, and –125 *dBc/Hz* respectively. Fig. 20 shows the simulated and measured phase noise plot for 0.05% tuning range of the CRO (shown in Fig.19). Theoretical prediction from both the noise model (negative resistance and feedback model) is in good agreement within 1-4 dB with the simulated (Ansoft Designer) and the measured results.

IV. MCLR VCO IMPLEMENTATION & VALIDATION

Based on the patent pending approach, traditional CROs can be replaced by a planar coupled distributed resonator in which a desirable resonant frequency can be adjusted with less deterioration in Q and less production process steps is characterized as a novel structure as MCLR, capable of operating at different fixed frequency in series, parallel and hybrid modes [8].

Figures 21 (a), (b), (c) depict the typical layout of fixed frequency (less than 0.1% tuning range) planar MCLR VCO; and (d) shows the measured phase noise plot for frequency 1000 MHz in series, parallel, and hybrid resonance mode. It can be seen from Figure 21 (d), hybrid resonance mode offers minimum phase noise but at the cost of higher order and spurious mode that may lead to stop the oscillation over the band (for > 0.1% tuning range).

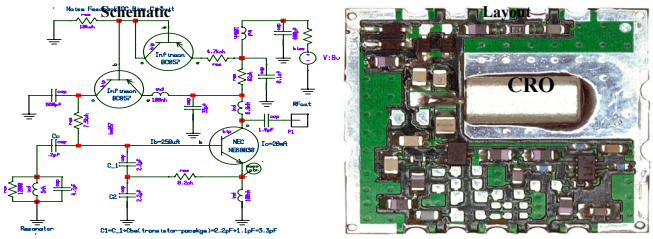

Fig. 19 1 GHz Colpitts oscillator (Ceramic resonator oscillator)

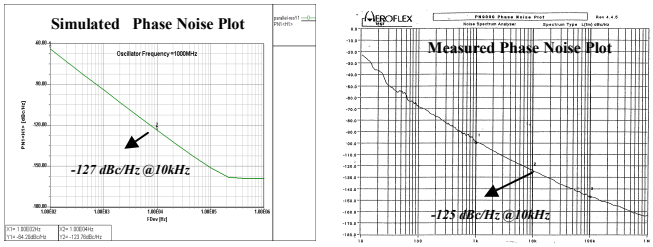

Fig. 20. Simulated and measured phase noise plot of for CRO (Fig. 19)

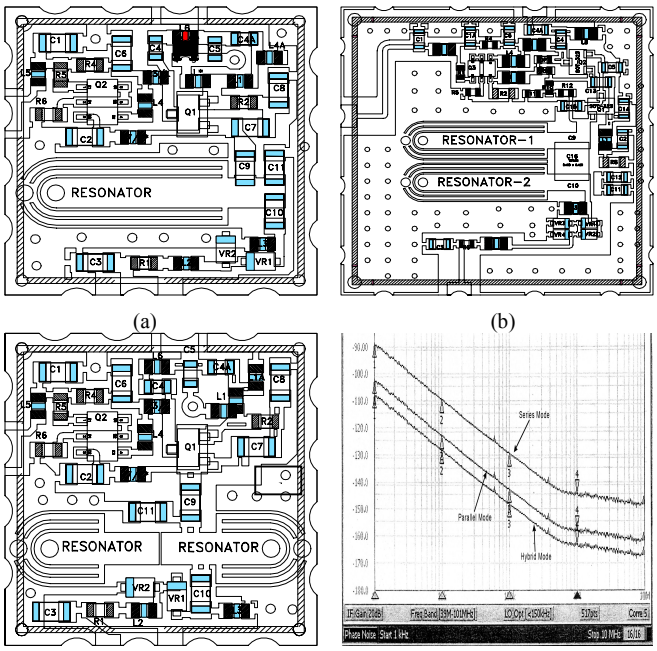

Fig. 21. (a) Series mode MCLR VCO, (b) Parallel mode MCLR VCO, (c) Hybrid mode MCLR VCO, (d) Measured phase noise plot

Figs. 22 and 23 show the block diagram and schematic of user-definable fixed frequency hybrid mode MCLR VCO (600-2500MHz) in which a series and parallel stubs (S_1, S_2 S_3, S_4, S_5, S_6 S_7, S_8) controls the dominant mode by incorporating feedback mechanism using dynamically gain stabilization and conduction angle network.

MCLR VCOs shown in Figure 21 offers cost-effective alternative to CROs but limited to less than 1% tunability. Figure 22 offers more than 1% (1-5%) tunability without degradation of the phase noise performance by dynamically tuning MCLR network for maximum group delay and sharper phase characteristics so that noise impedance transfer function is optimum for a given modes, and able to achieve optimum group delays matched to respective output signal frequencies for minimum noise.

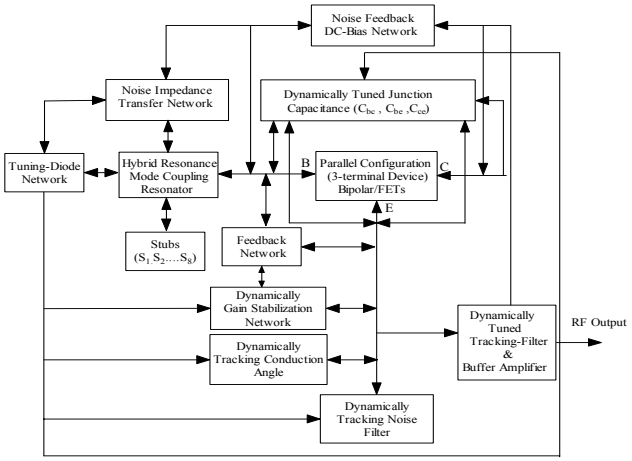

Fig.22. Block diagram of a user-definable MCLR VCO (600-2500 MHz)

The object of the present approach is to minimize and compensates the variation in the nonlinear junction capacitances (C_{bc}, $C_{be,,}$ and C_{ce}) of the transistor so that the same oscillator circuit can be used for the several different frequency bands (user definable) allocated for present and later generation wireless systems.

This may be accomplished by adding tunable capacitor across the junction capacitances of the transistor so that the influence of the junction capacitances (C_{bc}, $C_{be,,}$ and C_{ce}) can be reduced considerably due to change in the bias point, temperature, operating frequency, oscillator conduction angle, and drive level. The active part includes external linear capacitances (C_3, C_4 C_5, C_6 C_7, C_8) that are connected in parallel with each nonlinear junction capacitances (C_{bc}, $C_{be,,}$ and C_{ce}), which are integral part of the active device Q_1& Q_2 (Q_1,Q_2: parallel connected; AC or DC coupled, as shown in the circuit diagram in Fig.23). To achieve optimum results, the value of the linear capacitances (C_3, C_4 C_5, C_6 C_7, C_8) should be greater than the effective values of the corresponding junction capacitance for the given drive level, operating frequency, and bias conditions.

Fig.24 shows the layout of MCLR VCO, where resonators are positioned parallel to each other, in such a way that adjacent resonators are coupled along the guided length for the given frequencies. The layout shown in Fig. 17 is 6-layer board, fabricated on 64mil thick Roger substrate of dielectric constant 3.38 and loss tangent $2.7x10^4$. The choice of substrate depends on size, higher-order modes, surface wave effects, implementations (couplings, line length, width, spacing, and spacing tolerances), dielectric loss, temperature stability, and power handling (dielectric strength and thermal conductivity).

In an exemplary embodiment as shown in the Fig. 23, introducing a hybrid resonance mode-coupling and noise-impedance transfer network that causes a change in phase characteristics of the resonator network by modifying the transfer function towards steeper phase slope, thereby an increase in the effective dynamic loaded Q of the MCLR (Multi-coupled line resonator) network. In addition to this, patent pending topology as shown in Figures 22 and 23, offers user definable fixed frequency (600-2500MHz), and also suppress the higher order spurious mode, which is the main limitation of the tuning range for oscillator circuits shown in Figure 21.

Unfortunately each development design of VCO using planar MCLR has its price, since they occupy larger PCB area and for the same space exhibit much lower Qs compared to high Q, CRO/SAW resonator. For the most part, these disadvantages have been overcome by means of mode coupling approach, which acts as a Q-multiplier; and minimization of noise over the band is achieved by incorporating noise filtering network, noise cancellation network, phase compensating network, and noise feedback bias circuit [1-4].

The measured results provide more than 15-30dB improvements in the noise performance compared to the conventional microstripline resonator based oscillator and also supports minimum phase hits, and better phase noise performance than commercial available CROs at a fraction of cost (for a given frequency).

Figure 25 shows the measured phase noise plot for conventional microstrip resonator based VCO (prior art) and MCLR VCO (new approach) for frequencies 622 MHz, 1000 MHz, and 2488 MHz. The phase noise performance of MCLR VCO is better than 20-40 dB in comparison to conventional microstrip resonator based VCO; the measured phase noise performance for MCLR VCO @ 10kHz offset from the carrier, typical values: –138dBc/Hz (carrier frequency: 622MHz), –134dBc/Hz (carrier frequency: 1000MHz), and –128dBc/Hz (carrier frequency: 2488MHz); and is not limited to these frequencies. The circuit works at 8V, 30mA, and typical output power is 5dBm, and second harmonic rejection is better than –20dBc.

Figure 26 show the plot of the mesaured thermal drift for the oscillator circuits shown in Figures 19 (ceramic resonator based oscillator) and 23 (MCLR based oscillator) for 5% tuning range. From Figure 26, the MCLR VCO offers broadband tunability, extended operating temperature range in comapriosn to the traditional CROs, and overcome the limiting performance of the compensating frequency drift due to temperature, component tolernaces and ageing.

Figure 27 show the mesaured phase noise plot of the CROs and MCLR VCOs for frequency 622 MHz, 1000 MHz, and 2488 MHz with the 1-5% frequency tuning. For the same tuning range (1-5%), MCLR VCOs offer better phase noise performance in comparision to traditional CROs. With regard to the state-of-the-art, new planar MCLR VCOs offers cost-effective alternative to CROs and SAW (surface accoustic wave) resonator based oscillators for applications in modern wireless communication systems.

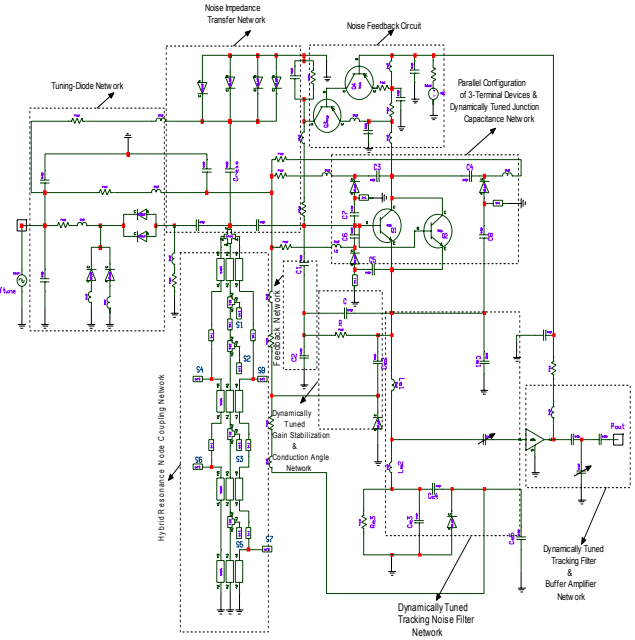

Fig.23. Schematic of user-defined MCLR VCO (Patent pending)

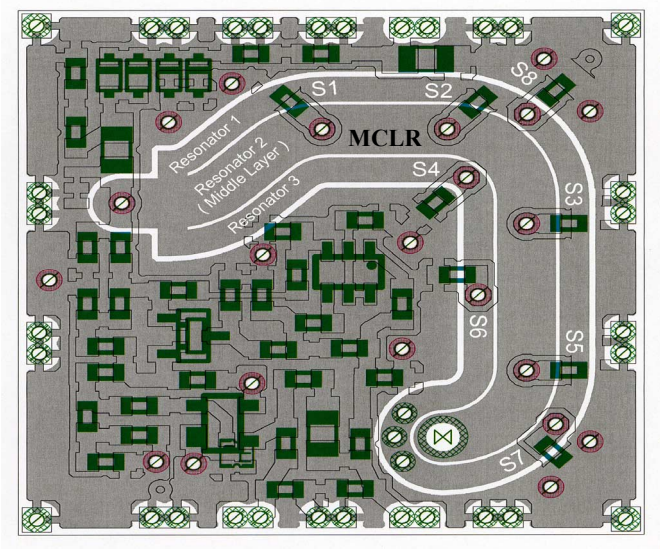

Fig.24. Layout of user-defined MCLR VCO (Patent pending)

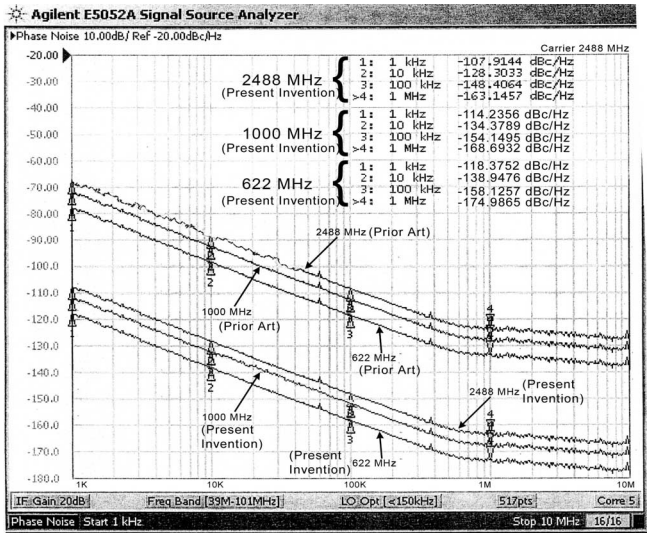

Fig. 25. Phase noise plot of planar resonator (prior art) and MCLR VCO

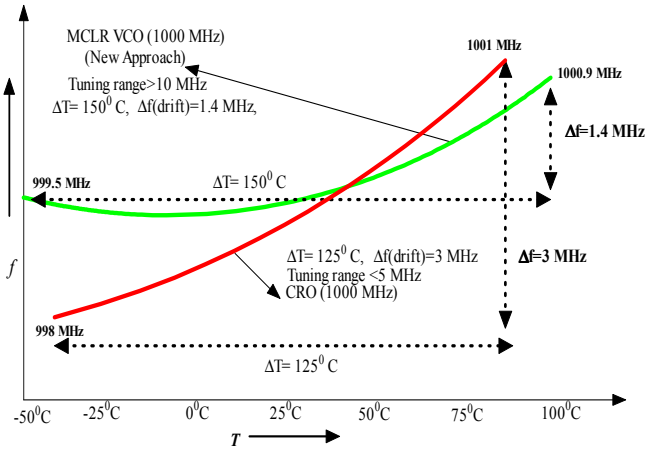

Fig.26. Measured thermal drift and frequency turning range (Δf) of conventional CROs and MCLR oscillators

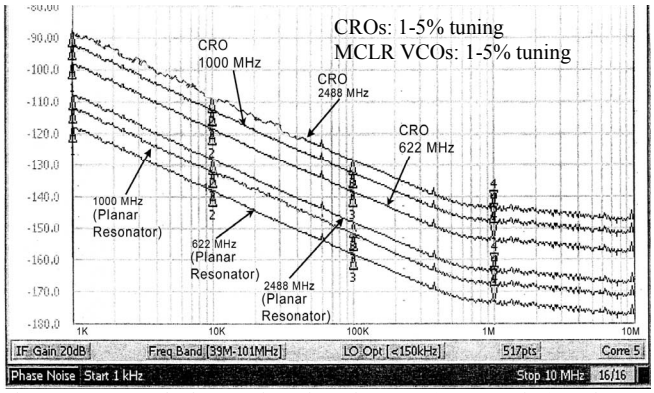

Fig. 27. Measured phase noise plot of CROs (1-5% tuning) and user-defined MCLR VCO (1-5% tuning)

V. CONCLUSION

With regard to the state of the art, novel MCLR replace traditional discrete and bulky ceramic/SAW resonators in oscillators/VCOs, and offer promising alternative for high Q planar resonators in the context of a planar fabrication process compatible with existing IC and MMIC processes.

REFERENCES

[1] A. K. Poddar, " A Novel Approach for Designing Integrated Ultra Low Noise Microwave Wideband Voltage Controlled Oscillators, "Dr.-Ing. Dissertation, TU- Berlin, Germany, 14 December 2004.

[2] U. L. Rohde, A. K. Poddar, J. Schoepf, R. Rebel, and P. Patel," Low Noise Low Cost Ultra Wideband N-Push VCO," *IEEE MTT-S, 2005.*

[3] U. L. Rohde, A. K. Poddar, and G. Boeck, *Modern Microwave Oscillators for Wireless Applications: Theory and Optimization*, John Wiley & Sons Inc., 2005.

[4] U. L. Rohde and A. K. Poddar, " Impact of Device Scaling on Phase Noise in SiGe HBTs UWB VCO*," IEEE, MTT-S* 2006, USA.

[5] U. L. Rohde and A. K. Poddar, " MEMS Enabled VCO for Wireless Connectivity," GigaHertz2005, Sweden, November 8-9, 2005.

[6] U. L. Rohde and A. K. Poddar, " An Analytical Approach of Minimizing VCO Phase Noise," APMC, China, December 4-7, 2005.

[7] U. L. Rohde and A. K. Poddar, " Configurable Ultra Low Ultra Wideband Power Efficient VCOs", 11th EUWC Cyprus, April 2005.

[8] U. L. Rohde, A. K. Poddar, and R. Rebel, " Ultra Low Noise Low Cost Octave-Band Hybrid-Tuned VCO," IEEE CCECE 05, Canada.

[9] U. L. Rohde and A. K. Poddar, " A Unified Method of Designing Low Noise Oscillator," International Microwave and Optoelectronics Conference (IMOC'2005), Brazil, July 25-28, 2005

[10] U. L. Rohde and A. K. Poddar, "Configurable Adaptive Ultra Low Noise Wideband VCOs," IEEE, ICU 2005, Switzerland.

[11] U. L. Rohde, K. J. Schoepf and A. K. Poddar, " Low-Noise VCOs Conquer Wide Bands", Microwave & RF, pp. 98-106, June 2004.

[12] U. L. Rohde, A. K. Poddar, and K. J. Schoepf " Cost-Effective VCOs Replace Power-Hungry YIGs", Microwave & RF, April 2006.

[13] S. Romisch, J. Kitching, E. S. Ferre-Pikal, L. Hollberg, and F. L. Walls, "Performance Evaluation of an Optoelectronic Oscillator", *IEEE Tran. Ultrason. Ferr.*, 47, Sept 2000, pp. 1159-1165.

[14] A. P. S (Paul) Khanna, "Microwave Oscillators: The State of The Thechnology", Microwave Journal, pp. 22-42, April 2006.

[15] J. De Los Santos, G. Fischer, H. A.C. Tilmans, and J. T. M. van Beek, "RF MEMS for Ubiquitous Wireless Connectivity " IEEE Microwave Magazine, pp, 36-49, December 2004.

[16] H. J. De Los Santos, "MEMS-A wireless vision, " Proc. Int. MEMS Workshop, Singapore, 2001, pp. 35-42.